Title

Secondary Organic Aerosol from OH-Initiated Oxidation of Mixtures of d-Limonene and β-Myrcene.

Journal

Environmental Science and Technology, 58(30)

Authors

Liu, Sijia

Galeazzo, Tommaso

Valorso, Richard

et al.

Publication Date

2024-07-17

DOI

10.1021/acs.est.4c04870

Peer reviewed

Environmental Science & Technology

pubs.acs.org/est

Article

Secondary Organic Aerosol from OH-Initiated Oxidation of Mixtures of D-Limonene and β-Myrcene

Sijia Liu, Tommaso Galeazzo, Richard Valorso, Manabu Shiraiwa, Celia L. Faiola, and Sergey A. Nizkorodov*

Cite This: *Environ. Sci. Technol.* 2024, 58, 13391−13401

Read Online

ACCESS | Metrics & More | Article Recommendations | Supporting Information

ABSTRACT: The chemical composition and physical properties of secondary organic aerosol (SOA) generated through OH-initiated oxidation of mixtures containing β-myrcene, an acyclic monoterpene, and D-limonene, a cyclic monoterpene, were investigated to assess the extent of the chemical interactions between their oxidation products. The SOA samples were prepared in an environmental smog chamber, and their composition was analyzed offline using ultraperformance liquid chromatography coupled with electrospray ionization high-resolution mass spectrometry (UPLC-ESI-HRMS). Our results suggested that SOA containing β-myrcene showed a higher proportion of oligomeric compounds with low volatility compared to that of SOA from D-limonene. The formula distribution and signal intensities of the mixed SOA could be accurately predicted by a linear combination of the mass spectra of the SOA from individual precursors. Effects of cross-reactions were observed in the distribution of isomeric oxidation products within the mixed SOA, as made evident by chromatographic analysis. On the whole, β-myrcene and D-limonene appear to undergo oxidation by OH largely independently from each other, with only subtle effects from cross-reactions influencing the yields of specific oxidation products.

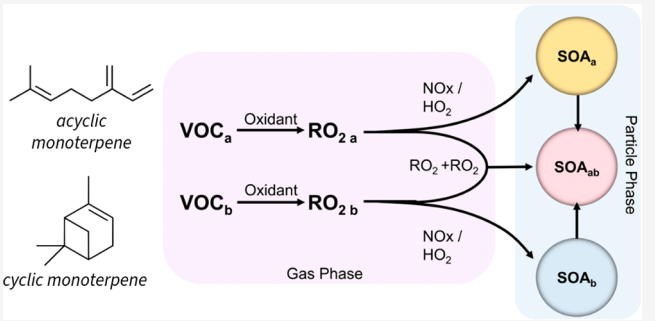

KEYWORDS: *cyclic monoterpene, acyclic monoterpene, stressed-plant emissions, cross-reaction product, oligomer, volatility, viscosity*

INTRODUCTION

Secondary organic aerosol (SOA) constitutes a substantial fraction of global atmospheric particulate matter,[1−3] contributing to the uncertainty of climate change predictions because of its complex effects on clouds and radiative forcing.[2−5] Generated primarily from atmospheric oxidation of volatile organic compounds (VOCs),[6−9] SOA plays an integral role in new particle formation (NPF) and growth,[8,10,11] cloud condensation,[12,13] visibility degradation,[14,15] chemical transformations of air pollutants,[10,11] and air quality.[16−18]

Biogenic volatile organic compounds (BVOCs), such as isoprene, monoterpenes, and sesquiterpenes, are plant-emitted secondary metabolites that constitute up to 90% of global VOC emissions and play a crucial role in the formation of SOA.[6,19−23] Environmental stressors and climate change significantly impact the quantity and composition of BVOC emissions.[6,24−27] Once released to the atmosphere, these highly reactive BVOCs engage in chemical interactions within a complex mixture of atmospheric compounds.[19−21,28] Mechanistic understanding of this chemistry has been explored in laboratory biogenic SOA studies that have largely focused on individual monoterpene oxidation, offering key insights into simplified atmospheric BVOC chemistry. However, evidence is accumulating that the chemistry of mixtures, which is more representative of the natural environment, can often deviate from predictions based on simple chemical systems. Mechanistic understanding of the chemical interactions between different BVOCs and their oxidation products, which is essential for SOA formation, remains uncertain. This ambiguity hinders accurate SOA representation in climate models, complicating the prediction of climate scenarios and the development of mitigation strategies.

In plant chamber experiments by Kiendler-Scharr et al., isoprene was found to suppress new particle formation (NPF) significantly, with the extent of the suppression increasing with the isoprene mixing ratios. This effect was attributed to the reduction in the concentration of hydroxyl radical (OH) by isoprene.[29] This mechanism for isoprene suppression of NPF could not explain field observations where the suppression was observed without any clear reduction of OH available for reaction.[30,31] In a follow-up study by the same group,

Received: May 15, 2024
Revised: July 9, 2024
Accepted: July 10, 2024
Published: July 17, 2024

McFiggans et al. maintained constant levels of OH in the chamber and showed that intermediates and products of isoprene oxidation reduced the formation of dimeric compounds from α-pinene by scavenging highly oxidized α-pinene peroxy radicals that would otherwise form dimers with low volatility.[32] This effectively increased the volatility of the oxidation products in the mixed system compared to α-pinene alone, which could mechanistically explain how a small acyclic BVOC like isoprene could suppress NPF in an environment containing a mixture of isoprene and monoterpenes. Nonlinear mixture effects have also been investigated in a few other BVOC chemical systems.[33−35] Dada et al. investigated the effects of sesquiterpenes in the mixture of α-pinene and isoprene and found that the addition of sesquiterpene to the mixture counteracted the scavenging effects of isoprene and increased the low volatility organic compound formation and NPF efficiency.[36] Takeuchi et al. conducted chamber experiments on NO_3 oxidation of α-pinene and D-limonene mixtures and observed that the yield of α-pinene oxidation products was enhanced by the presence of D-limonene, and conversely, the yield of D-limonene oxidation products was suppressed, suggesting nonlinear chemical effects in these mixed VOC systems.[37] Taken together, these previous studies emphasize the significant role of different types of VOC interactions in SOA formation, hinting at the complex nonlinear mixture effects at play. They collectively highlight the need for an in-depth understanding of these interactions to accurately represent SOA formation in atmospheric models.

This work aims to elucidate the chemical interactions taking place during the oxidation of mixtures of acyclic and cyclic monoterpenes, with an emphasis on the response of plants to stress factors including heatwaves, insect outbreaks, and drought leading to increased acyclic terpene emissions.[19,38,39] Faiola et al. demonstrated the tendency of acyclic terpene to fragment into smaller ($<C_{10}$) products during oxidation, especially ozonolysis.[40] Ylisirniö et al. observed similar effects of β-farnesene, an acyclic sesquiterpene, attributing to the exocyclic C=C bond scission during oxidation.[41] Given the fact that isoprene can change the SOA monomer/dimer distribution and thus the SOA formation,[29,32,42] we speculated that the small primary oxidation products from acyclic monoterpenes oxidation, such as β-myrcene, could have a similar suppressing effect.[43] Therefore, we hypothesized that smaller products of β-myrcene oxidation may also alter the dimeric compounds of SOA from D-limonene (Figure 1) by a mechanism similar to that presented in McFiggans et al.[32] We additionally postulated that interactions between acyclic β-myrcene and cyclic D-limonene oxidation products may yield distinct SOA formation mechanisms, impacting SOA composition and properties, such as viscosity and volatility.[44,45] To probe the potential cross-reaction between oxidized products of D-limonene and β-myrcene and compare the composition of SOA generated via photooxidation of different VOC mixtures with the presence of OH, we utilized offline UPLC-ESI-HRMS to examine the distribution of oxidation products in mixtures with different initial compositions of β-myrcene and D-limonene. Our study underscores the complexity of BVOC mixture oxidations and emphasizes the necessity for further investigation.

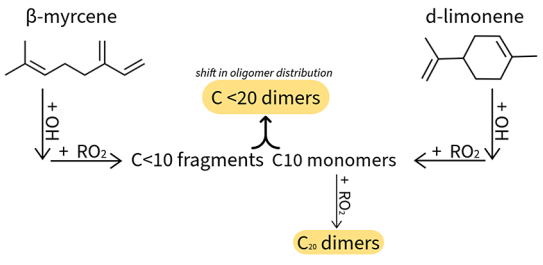

Figure 1. Fragmentation resulting from β-myrcene oxidation could hypothetically alter the product distribution in the mixture, favoring smaller carbon numbers in the backbone compared to those in pure D-limonene SOA.

METHODS

Chamber Experiments. SOA was generated in a 5 m^3 Teflon PFA environmental smog chamber via OH-initiated photooxidation. Before each experiment, the chamber was thoroughly cleaned for 12 h by UV-irradiating air containing parts per million levels of O_3 and H_2O_2 at ∼100% relative humidity (RH). The chamber was then flushed with zero air to remove the products of cleaning, resulting in undetectable levels of residual particles. The chamber was reconditioned to ∼50% RH with an air humidifier (Perma Pure FC125) and room temperature (20 ± 1 °C) for SOA generation. D-limonene (Thermal Fisher, 97% purity, stabilized) and/or β-myrcene (Sigma-Aldrich, purity 93.5%, Lot # BCBS9813 V) were injected into the chamber by evaporating microliter quantities (1−2 μL) of pure compounds into a flow of heated air (2 L min^{-1} at ∼45 °C), followed by injection of 45 μL of 30 wt % H_2O_2 to provide ∼2 ppm of H_2O_2 vapor to serve as a precursor for OH. The initial mass concentrations of D-limonene and β-myrcene are summarized in Table 1. The experimental approach was designed to keep the overall reactivity with OH the same for all mixtures, i.e., keeping $k_{OH+LIM}[LIM] + k_{OH+MYR}[MYR]$ constant. As a result, the starting concentration of β-myrcene is intentionally lower than that of D-limonene in Table 1, in order to account for β-myrcene's higher rate constant for OH reaction (k_{OH+MYR} = 2.15 × 10^{-10} cm^3 s^{-1} mol^{-1}), compared to that of D-limonene (k_{OH+LIM} = 1.64 × 10^{-10} cm^3 s^{-1} $molecule^{-1}$).[46] However, the steady-state OH level turned out to be different for different monoterpene mixtures (see below), making the overall rate of monoterpene change by up to a factor of 2, depending on the mixture composition. For mixed-VOC experiments, D-limonene was injected into the chamber first, followed by β-myrcene. Proton-transfer-reaction time-of-flight spectrometry (PTR-ToF-MS; IONICON model 8000) was used to verify that the mixing ratios of monoterpenes reached a stable level by monitoring the m/z 137 signal corresponding to protonated monoterpenes. Air samples were collected using multibed stainless steel adsorbent cartridges to measure monoterpene concentrations before and after photooxidation, and subsequently analyzed via thermal-desorption coupled to gas chromatography−mass spectrometry (TD-GC−MS). Detailed sampling and analysis procedures are provided in the Supporting Information.

To initiate SOA generation, a bank of UV−B light was turned on. PTR-ToF-MS was used to monitor the rate of monoterpene consumption to estimate the steady-state concentration of OH. The estimated average number concentrations of OH for pure β-myrcene and D-limonene experiments were 1.93 × 10^6 and 3.85 × 10^6 cm^{-3}, respectively. The OH should reach a photostationary state in a chamber containing only H_2O_2 but the presence of reactive monoterpenes reduces the steady-state OH concentration, and

https://doi.org/10.1021/acs.est.4c04870
Environ. Sci. Technol. 2024, 58, 13391−13401

Table 1. Summary of Chamber Experiments: Starting Mass Concentrations of β-Myrcene and D-Limonene, Change in Total Monoterpene Mass Concentration during Photooxidation, Amount of SOA Produced, SOA Yield, Monomer/Oligomer Ratio, and Average O/C Ratio in the SOA

precursors	starting β-myrcene ($\mu g/m^3$)	starting D-limonene ($\mu g/m^3$)	fraction of OH reactivity due to β-myrcene (%)	total VOC reacted, ΔVOC ($\mu g/m^3$)	ΔSOA ($\mu g/m^3$)	SOA yield	monomer fraction in SOA (%)	average O/C in SOA
D-limonene	0	688 ± 45	0	688 ± 45	224 ± 37	0.33 ± 0.05	67.1	0.45
β-myrcene	412 ± 72	0	100	412 ± 72	269 ± 45	0.65 ± 0.16	53.3	0.52
β-myrcene + D-limonene	172 ± 17	189 ± 19	54.5	361 ± 26	193 ± 32	0.53 ± 0.10	61.7	0.49
β-myrcene + D-limonene	312 ± 45	97 ± 14	80.8	378 ± 47	308 ± 51	0.81 ± 0.17	56.7	0.50
β-myrcene + D-limonene	190 ± 17	246 ± 21	47.9	399 ± 26	267 ± 45	0.67 ± 0.12	61.9	0.50
β-myrcene + D-limonene	124 ± 12	188 ± 19	46.3	283 ± 23	296 ± 49	1.04 ± 0.19	64.6	0.49
β-myrcene + D-limonene	87 ± 8	294 ± 30	28.0	347 ± 31	224 ± 37	0.65 ± 0.12	63.5	0.48
β-myrcene + D-limonene	369 ± 18	167 ± 12	19.6	372 ± 22	270 ± 45	0.72 ± 0.13	61.5	0.46

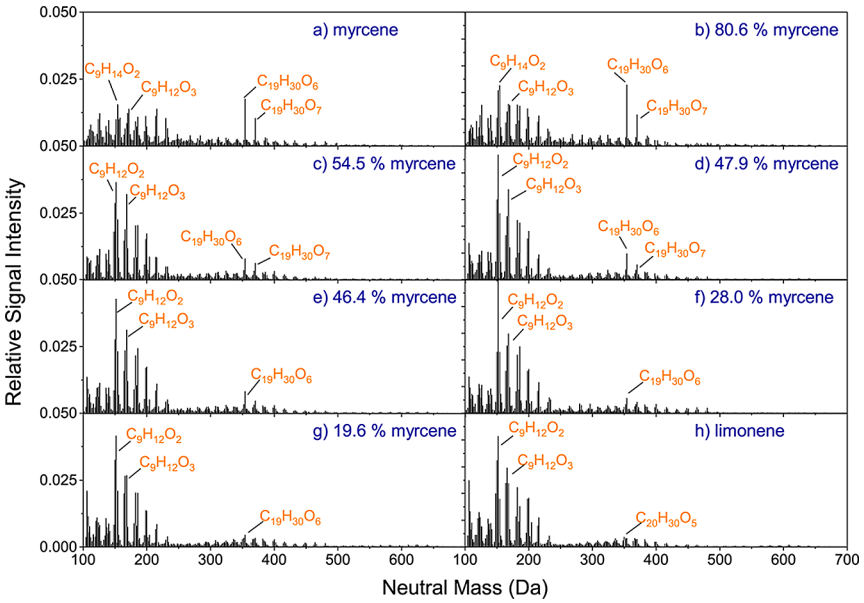

Figure 2. High-resolution mass spectra (100−700 Da) of SOA produced from mixtures of β-myrcene and D-limonene. Each panel represents a different starting VOC system and is labeled by the fractional OH reactivity contributed by β-myrcene (a) pure β-myrcene, (b) 80.6% β-myrcene, (c) 54.5% β-myrcene, (d) 47.9% β-myrcene, (e) 46.4% β-myrcene, (f) 28.0% β-myrcene, (g) 19.6% β-myrcene, and (h) pure D-limonene. Major peaks in each spectrum are labeled with their respective assigned chemical formula.

the reduction is larger for β-myrcene because its first-generation products have higher reactivity toward OH. The particle number concentration and size distribution were measured with a scanning mobility particle sizer (SMPS; TSI, Inc.), consisting of an electrostatic classifier, a differential mobility analyzer (DMA; model 3080), and a condensation particle counter (CPC; model 3775). After the concentration of particles reached ∼250 $\mu g/m^3$ (approximately 2 h into photooxidation), the UV−B lights were turned off. Another set of adsorbent cartridge samples was collected to confirm that all of the monoterpenes reacted within the measurement uncertainties (Table 1). After that, SOA was collected on a Teflon filter (Fluoropore 0.2 μm PTFE hydrophobic nonsterile membrane) at a flow rate of ∼20 L min^{-1} for ∼3 h. The filter was weighed using a microbalance (Sartorius ME-5F, 1 μg precision) before and after the collection, sealed, and stored in a freezer (∼−20 °C) before offline analysis. SOA filter samples were then analyzed using UPLC-ESI-HRMS, with molecular formula assignments to the detected mass spectra peaks using MFAssignR.[47] Detailed extraction and analysis methods are provided in the Supporting Information.

GECKO-A Mechanism Modeling. The Generator for Explicit Chemistry and Kinetics of Organics in the Atmosphere (GECKO-A)[48] was used to generate reaction mechanisms for the photooxidation of D-limonene, β-myrcene, and the mixture of the two species. Since GECKO-A does not treat autoxidation nor the ROOR formation pathway, GECKO-A was primarily used for $[HO_2]/[RO_2]$ predictions. In addition, the top 2000 predicted products were used for estimating isomer diversity among different reaction systems. The detailed GECKO-A parameters and methods are included in the SI. Importantly, the simulations predicted the number concentrations of HO_2 (1.3×10^8, 3.8×10^8, 7.5×10^7 cm^{-3} for D-limonene, β-myrcene and the mixture case, respectively) and all RO_2 radicals combined (4.4×10^9, 9.7×10^9, 1.1×10^{10} cm^{-3}) after 2 h oxidation in the chamber. The rate constants for $RO_2 + HO_2$ reactions are on the order of 10^{-11} cm^3 s^{-1}, and rate constants for $RO_2 + RO_2$ reactions range from 10^{-13} cm^3 s^{-1} for less oxidized RO_2 to 10^{-11} cm^3 s^{-1} for more oxidized RO_2.[49] These concentrations and rate constants suggest that $RO_2 + R'O_2$ reactions played an important role in controlling the fate of RO_2 in the chamber and presumably contributed to the dimer formation.

https://doi.org/10.1021/acs.est.4c04870
Environ. Sci. Technol. 2024, 58, 13391−13401

RESULTS AND DISCUSSION

High-Resolution Mass Spectra. The mass spectra of the SOA formed from eight different chemical systems representing a range of β-myrcene:D-limonene ratios are shown in Figure 2. The major detected formulas for all the reaction systems are dominated by C_9 compounds. However, the most common monoterpene monomer products observed in previous laboratory experiments and field work are C_{10} compounds.[50,51] Extracted ion chromatograms (EICs) for the top C_9 ions across all systems displayed broad, unresolved peaks, indicating that at least some of the C_9 ions must have formed by fragmentation of ions from multiple eluting SOA compounds (Figure S3).

To avoid ion fragmentation issues, we focus our attention on the major C_{10} monomer and C_{19-20} dimer compounds observed in the different reaction systems, as these groups are consistently identified in previous monoterpene mass spectra.[50−52] The $C_{10}H_{16}O_x$ and $C_{10}H_{14}O_x$ families represent the most abundant compounds observed across SOA from various mixtures, which is attributable to the fact that β-myrcene and d-limonene are isomers. Specifically, for β-myrcene, the predominant C_{10} monomers are $C_{10}H_{16}O_5$, $C_{10}H_{14}O_4$, and $C_{10}H_{14}O_6$, listed in order of decreasing abundance. Conversely, D-limonene SOA displays a less oxygenated profile of the top C_{10} monomers, including $C_{10}H_{14}O_2$, $C_{10}H_{14}O_3$, and $C_{10}H_{16}O_4$. Reducing the proportion of β-myrcene in the precursor mixture results in a shift toward D-limonene's formula products as the dominant C_{10} monomers, as depicted in Figures 2 and S4. The observed dominant dimer families among all of the SOA are $C_{19}H_{30}O_x$, $C_{20}H_{30}O_x$, and $C_{20}H_{32}O_x$ (Figures 2 and S5). The $C_{20}H_{30}O_x$ dimers likely form from $C_{10}H_{15}O_x$ + $C_{10}H_{15}O_y$ dimerization reactions, whereas $C_{20}H_{32}O_x$ may result from reactions between $C_{10}H_{15}O_x$ and $C_{10}H_{17}O_x$ radicals, the major $C_{10}-RO_2$ species in monoterpene oxidation.[52] C_{19} dimers presumably emerge from C_9 and $C_{10}-RO_2$ radical cross-reactions or via RO_2-RO_2 reactions followed by the loss of CH_2O. In terms of the relative abundance of the monomer and dimer products, in the case of pure β-myrcene SOA, approximately 45% of the peak abundance originated from dimeric ($10 < \#C \leq 20$) and larger ($\#C > 20$) components. The oligomer signals identified in D-limonene SOA were smaller and accounted for 30% of the total signal abundance (Table 1). As the fraction of β-myrcene in the mixture increases, as shown in Figure 2, the proportion of oligomers also increases.

McFiggans et al. compared the monomer/dimer ratio in α-pinene SOA formed in the presence and absence of isoprene and found that the dimer to monomer ratio was decreased by nearly a factor of 3 in the presence of isoprene, small and highly reactive, illustrating the product scavenging effect.[32] Contrary to expectations that the primary oxidation products of acyclic β-myrcene would shift the monomer/dimer distribution in SOA mass spectra toward lower molecular weights (Figure 1), β-myrcene in the mixture did not impede the formation of high molecular weight compounds essential for SOA particle formation. Instead, SOA from β-myrcene exhibited a higher proportion of dimeric compounds than did SOA from D-limonene. Furthermore, a consistent progression in the ratio of monomers to dimers was observed in the SOA mass spectra, transitioning smoothly from systems dominated by β-myrcene to systems dominated by D-limonene. This implies that β-myrcene does not efficiently fragment during OH oxidation to form smaller oxidation products that would otherwise act as SOA scavengers. Therefore, the inhibition of dimer formation by isoprene observed by McFiggans et al. cannot be generalized to acyclic monoterpenes such as β-myrcene, despite their previously noted propensity to fragment during oxidation.

The mass spectra of SOA generated from all precursor systems were dominated by the same set of formulas, with some small variation in peaks observed between different systems. The UpSet plots in Figure 3 help illustrate the level of

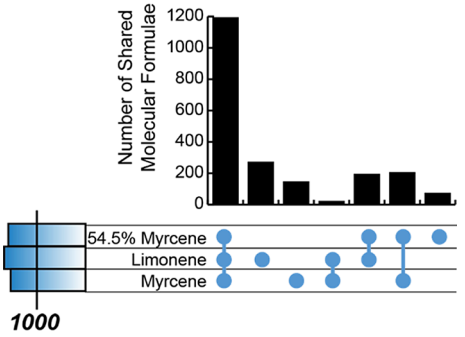

Figure 3. UpSet plots for comparing overlap among molecular formulas detected in 54.5% β-myrcene (mixture), β-myrcene, and D-limonene SOA as identified by HRMS. The horizontal bar charts at the bottom left display the total number of unique chemical formulas or structural formulas in each system. The matrix illustrates the intersections between systems through filled blue circles. The vertical bar chart quantifies the number of these intersections. Each data point was only counted once. For example, the leftmost vertical bar in panel, with all circles filled, indicates 1193 shared formulas across all three SOA systems, whereas the second bar represents 271 formulas unique to the D-limonene SOA.

overlap in the formula distributions. The combined set of assigned formulas for 54.5% β-myrcene (mixture), β-myrcene, and D-limonene SOA had 1665 species. Of those, 1193 formulas were common to all three SOA systems, and 73 chemical formulas were only observed in the mixture SOA, constituting less than 5% by peak number and less than 1% by the integrated peak abundance in the mass spectra. Figure 3 implies that cross-reactions between β-myrcene and D-limonene oxidation products (including reactions of peroxy radicals) do not form a large number of unique formulas. However, the overlapping formula distributions can be ambiguous, as they do not account for the isomerism of the observed compounds (see below). Indeed, the GECKO-A modeling results suggest that there could be up to 75 isomeric products for a single chemical formula product (Figure S6).

Modeling Mixture SOA As a Linear Combination of Individual SOA. Takeuchi et al. conducted chamber experiments with a mixture of α-pinene and D-limonene in the presence of nitrate radicals (NO_3).[37] They observed that additional α-pinene resulted in an increased abundance of monomeric products in the resultant SOA compared to the SOA formed from only D-limonene, which could not be simply explained by linear addition. We also tested how well the mass spectra of SOA from the mixed VOC experiments can be modeled as a linear combination of mass spectra from experiments for individual VOCs. Figure 4 compares observed peak abundances in mass spectra of SOA prepared from VOC mixtures on the *x*-axis and peak abundances obtained from a linear combination of peak abundances in mass spectra of

https://doi.org/10.1021/acs.est.4c04870
Environ. Sci. Technol. 2024, 58, 13391−13401

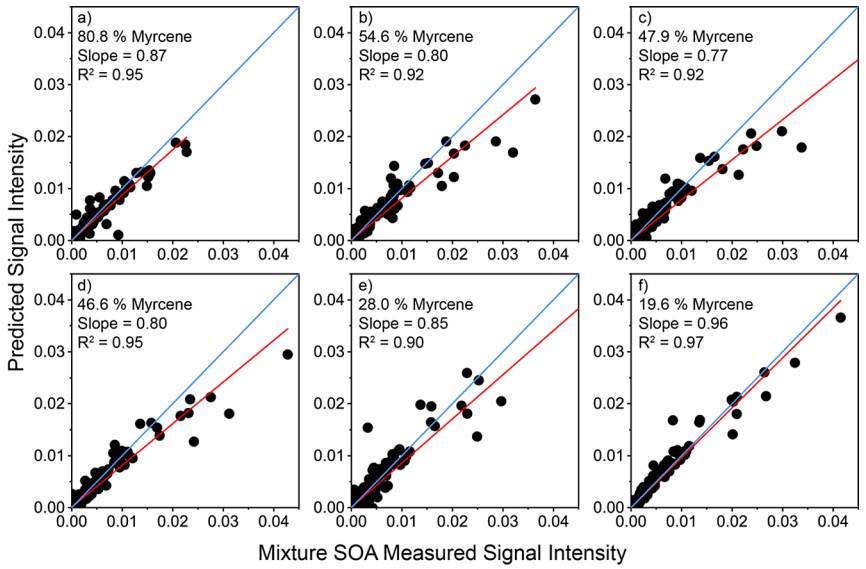

Figure 4. Comparison between HRMS peak abundance of linear addition prediction and observed mixture SOA. The blue line is plotted to serve as the 1:1 reference line. This line would signify perfect agreement between the predicted and observed values. The red line represents a linear regression through the actual data.

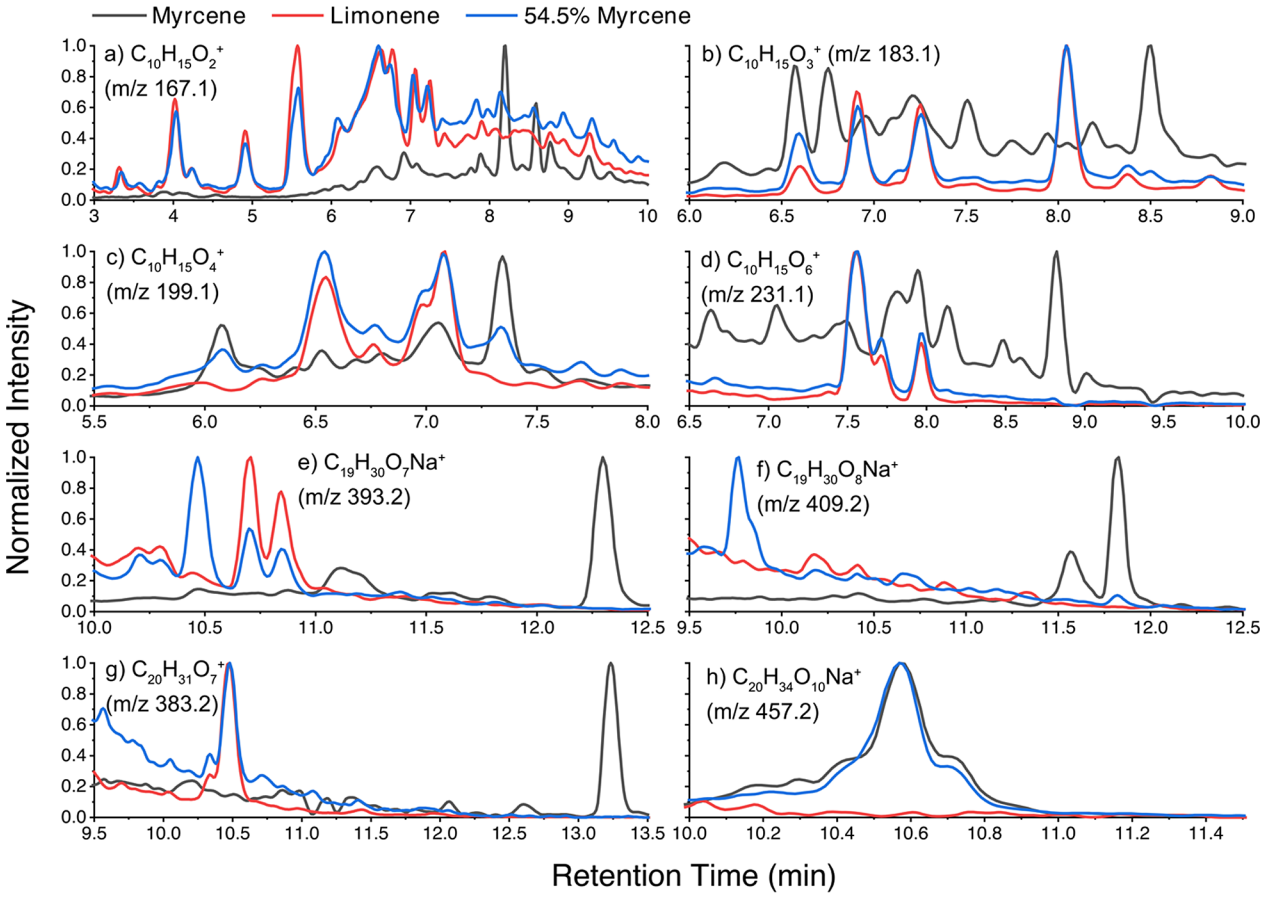

Figure 5. EICs displaying the ion abundance observed for (a) $C_{10}H_{15}O_2^+$, (b) $C_{10}H_{15}O_3^+$, (c) $C_{10}H_{15}O_4^+$, and (d) $C_{10}H_{15}O_6^+$ monomeric and (e) $C_{19}H_{30}O_7Na^+$, (f) $C_{19}H_{30}O_8Na^+$, (g) $C_{20}H_{31}O_7^+$, (h) $C_{20}H_{34}O_{10}Na^+$ dimeric ions of β-myrcene (black lines), 54.5% β-myrcene (blue lines), and D-limonene (red lines) SOA. Each panel represents comparative signal abundance across three different SOA sample types.

predictions of the glass transition temperature and viscosity of organic aerosols from volatility distributions d-limonene and β-myrcene SOA, based on their concentration ratio. If the predicted signal intensity from the linear combination aligns with the measured intensity of compounds within the SOA mixture, the resulting plot would exhibit a slope of 1 with minimal scattering. Compounds whose signal is either amplified or diminished due to mixing would be positioned

https://doi.org/10.1021/acs.est.4c04870
Environ. Sci. Technol. 2024, 58, 13391−13401

above or below the 1:1 line, respectively. Additionally, any shift in the dimer or monomer pattern resulting from cross-reactions would be evident.

The linear combination predicted the peak abundances in the mass spectra of mixed SOA with the slopes varying from 0.77 to 0.96 and R^2 values ranging between 0.90 and 0.97, suggesting a good correlation between our predicted and observed values. The closest agreement was observed for 19.6% β-myrcene SOA, with a slope of 0.96, close to the 1:1 line. For the other cases, the predicted peak abundances fell slightly below the 1:1 line, with slopes around 0.8−0.9, but the linearity was maintained, as indicated by unchanged R^2 values. Overall, we observed no significant nonlinear relationship between the predicted and measured signals, with the monomer and dimer patterns remaining consistent.

Extracted Electron Ion Chromatograms. The similar monomer/dimer pattern and the highly overlapping formula distribution across the SOA from different precursor systems obscured the possible mixture-specific products from cross-reaction between β-myrcene RO_2 and D-limonene RO_2. Therefore, we turned to UPLC data, which can separate isomeric compounds in SOA by their polarity.[53] Here, we examine the extracted electron ion chromatograms (EICs) of the top monomer and dimer products of β-myrcene, D-limonene, and mixture SOA. When comparing the major detected ions and the EICs of $C_{10}H_{14}O_x$ and $C_{10}H_{16}O_x$ monomer families, we observed that the majority of EICs for the mixture-derived SOA predominantly resemble a composite of the EICs observed in the D-limonene and β-myrcene SOA (Figures 5a−d and S7), that is to say, no major new monomeric peaks appear in the mixed SOA case. It should be noted, however, that the chromatograms do not simply add up: peaks from one of the monoterpenes tend to dominate the pattern. For example, the detected ion for $C_{10}H_{14}O_6$ ($C_{10}H_{15}O_6^+$, m/z 231.1) in the mixture-derived SOA, shows a similarity to the EIC of $C_{10}H_{15}O_6^+$ observed in the D-limonene SOA, whereas the corresponding pattern from the β-myrcene SOA is notably absent. This implies that while no new monomeric compounds form in the mixed SOA case, the yields of the monomeric peaks do change.

To further investigate the cross-reactions, we examined the EICs of the top dimer products, which may form through the RO_2−$R'O_2$ accretion pathway. Figures 5e−g and S8 illustrate the EICs for the primary C_{19} and C_{20} dimer products. Unlike EICs of monomers, the dimer EICs show not only a blend of D-limonene and β-myrcene SOA EICs but also traces of distinct new isomers in the mixture SOA. For example, the most prominent peak of $C_{19}H_{30}O_7$, detected as $C_{19}H_{30}O_7Na^+$, presents a distinct isomer in the mixture-derived SOA, eluting at approximately 10.48 min, absent in both D-limonene and β-myrcene SOA (Figure 5e). Similarly, the distinct peak at 9.75 min for the EIC of $C_{19}H_{30}O_8Na^+$, in the mixture of SOA signifies the cross-reaction producing a unique isomer of $C_{19}H_{30}O_8$ (Figure 5f). In addition, an inhibition of certain isomeric compounds in the mixture SOA was also observed for dimeric compounds. For example, EICs of $C_{19}H_{30}O_7Na^+$ of β-myrcene SOA have a strong peak at a retention time of 12.5 min that is absent from the SOA from the mixture SOA. We can therefore conclude that a complex interplay of interactions may occur during the oxidation of the VOC mixture, including both the suppression of specific pathways and the formation of new accretion products.

Volatility and T_g Estimation of BVOC Mixture SOA. Volatility and viscosity are important properties of SOA. They affect particle growth and evaporation kinetics, diffusion rates inside the particles, and atmospheric chemistry of compounds trapped inside the particles, including heterogeneous and multiphase reactions.[54−59] We estimated the pure compound saturation mass concentration (C_0) of each observed compound, calculated using the parametrization by Li et al.[60] (see detailed parametrizations in the SI). Figure 6 depicts the

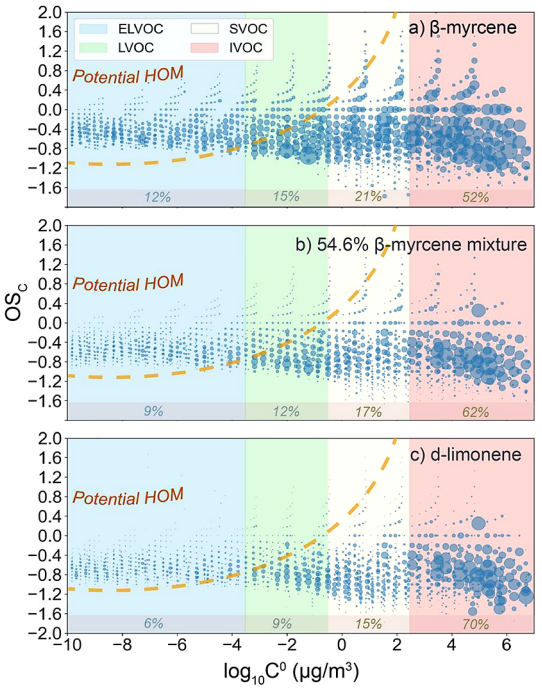

Figure 6. Relationship between average carbon oxidation state (OS_C) and the logarithm of the saturation concentration ($\log_{10} C_0$) for (a) β-myrcene, (b) 54.6% β-myrcene, and (c) D-limonene SOA. The bubble size is correlated with the detected peak abundance in the mass spectrum. Each plot displays a distribution of HRMS detected compounds classified into four volatility categories: extremely low volatility organic compounds (ELVOC; $C_0 < 3 \times 10^{-4}$ $\mu g/m^3$), low-volatility organic compounds (LVOC; $3 \times 10^{-4} < C_0 < 0.3$ $\mu g/m^3$), semivolatile organic compounds (SVOC; $0.3 < C_0 < 300$ $\mu g/m^3$), and intermediate volatility organic compounds (IVOC; $300 < C_0 < 3 \times 10^6$ $\mu g/m^3$). The orange dashed line indicates the area where highly oxygenated molecules are likely to be found based on their oxidation state and low volatility. The percentage of compounds in each category is also labeled at the bottom of each figure.

relationship between the average carbon oxidation state (OS_C) and volatility classes. It was observed that the SOA from β-myrcene contained a larger portion of its signal classified as ELVOC and LVOC compared to that from d-limonene SOA. Furthermore, as the concentration of β-myrcene in the mixture decreased, there was a notable decrease in the ELVOC and LVOC fractions, with an increase in the SVOC fraction, alongside a general decrease in the oxygen-to-carbon (O/C) ratio.

In our volatility predictions, we observed a substantial presence of IVOCs (generally corresponding to low-molecular-weight compounds with low O/C ratios). Given their high volatility, these compounds are not expected to reside in the particle phase, even under the relatively high mass loading ($\sim 10^2$ μg m^{-3}) in the chamber. While ESI-HRMS is

https://doi.org/10.1021/acs.est.4c04870
Environ. Sci. Technol. 2024, 58, 13391−13401

considered a "soft-ionization" technique, some ion fragmentation does take place in the ion source. This means that some of the IVOC signals must have originated from the fragmentation of larger oligomers, rather than being inherently present in the SOA. Therefore, we excluded compounds with C_0 larger than 10^2 $\mu g\ m^{-3}$ from the viscosity calculations described below.

We characterized the viscosity using the glass transition temperature T_g, which represents the temperature at which a transition to a glassy solid state occurs in a material. T_g was calculated for all detected compounds from their molecular formulas using the parametrizations by DeRieux et al. and Li et al.[61,62] (see the SI). Excluding the IVOC with $C_0 > 10^2$, the estimated viscosity for different SOA estimated for the experimental conditions (i.e., around 50% RH) ranges from 4.0×10^{11} to 5.3×10^{10} Pa s (Figure S9). Notably, SOA from pure β-myrcene and mixtures exhibits the higher viscosity characteristic of a semisolid material. With an increased fraction of D-limonene in the precursor mixture, there is a general trend of decreasing T_g and viscosity.

This observed pattern aligns with the results of Jokinen et al., who reported a substantially higher ELVOC formation from the oxidation of acyclic or exocyclic monoterpenes initiated by OH, compared to cyclic terpenes.[63] OH oxidation of both cyclic and acyclic bonds begins by adding an OH to the double bond, generating a peroxy radical. The key difference is that RO_2 radicals from acyclic terpenes are more flexible and have more available hydrogen atoms for intramolecular isomerization than d-limonene, making them more likely to form highly oxygenated organic molecules (HOMs).[64] The possibility of HOM loss during sample handling and mass spectrometry detection is noted.[65,66] Figure 6 highlights the potential HOM regions, where the β-myrcene-derived SOA exhibits a greater fraction of potentially detected HOMs in this region compared to all other examined SOA, and a decrease in the fraction of β-myrcene within the mixture precursors correlates with a reduction in the potential HOM signal. For β-myrcene, some of the RO_2 isomerization channels are expected to be especially favorable because of the allylic radical stabilization of the isomerization product (Figure S10). This stabilization could facilitate a more efficient autoxidation process, possibly leading to a higher yield of ELVOCs and a greater oxidation level in β-myrcene-derived SOA. In conclusion, the findings from this section indicate that pure β-myrcene SOA has lower volatility, higher viscosity, and greater oxidation compared to β-myrcene mixture SOA and d-limonene SOA.

SOA Yield. SOA yield is an important parameter describing the efficiency and extent of SOA formation from different precursor VOCs. The apparent SOA yields for all the cases studied here are included in Table 1 and Figure S11. For single precursor systems, β-myrcene exhibited almost double the SOA yield compared to D-limonene, 0.65 ± 0.16, and 0.33 ± 0.05, respectively. The SOA yield data in Figure S11 are relatively noisy but there is a clear trend for increasing the yield with an increased fraction of β-myrcene reactivity in the β-myrcene/D-limonene mixtures. As discussed above, the radical stabilization may contribute to β-myrcene's higher yield of ELVOC and LVOC, making it more efficient at making SOA. The scatter in SOA yield might be due to the inconsistency of starting VOC concentrations, which resulted in different amounts of SOA produced in the chamber leading to differences in the efficiency of gas-particle partitioning.[67] It is important to emphasize that specific measurements for the SOA yield to assess the comparative and conclusive influence of the mixture effect were not within the scope of our analysis, leaving the detailed investigation of this aspect for future work.

ATMOSPHERIC IMPLICATIONS

Ozonolysis of acyclic monoterpenes readily breaks them into smaller fragments compared to ozonolysis of cyclic monoterpenes with endocyclic C=C bonds.[40] Unlike ozonolysis, which breaks the C=C bonds, the OH oxidation is initiated by the addition of OH to the C=C bonds, followed by the usual RO_2/RO chemistry. While C−C bond scission in RO radicals from acyclic monoterpenes could lead to fragmentation as well, our work suggests that this fragmentation is relatively insignificant during OH-oxidation of β-myrcene. The extended and flexible skeleton of RO_2 radicals formed in the OH-oxidation of β-myrcene may afford efficient isomerization of these RO_2 radicals, leading to highly oxidized low-volatility products. In fact, β-myrcene forms SOA in a higher fraction of low-volatility dimeric products than SOA from OH oxidation of D-limonene, a cyclic monoterpene.

The lack of efficient fragmentation in the OH-oxidation of β-myrcene means that its primary oxidation products are not going to suppress SOA formation from other monoterpenes, as happens for isoprene. Both isoprene and longer acyclic monoterpenes, such as β-myrcene, have high reactivity toward OH ($k_{OH+ISO} = 1.01 \times 10^{-10}$; $k_{OH+MYR} = 2.15 \times 10^{-10}$ $cm^3\ s^{-1}$).[46] However, the products of isoprene oxidation, including cross-reaction products between isoprene and monoterpenes, are more volatile compared with the corresponding products from β-myrcene. Whereas there is a detectable suppression effect in the OH oxidation of the isoprene + α-pinene mixture,[29,32] there is no observable suppression in the β-myrcene + D-limonene case.

Another implication of this work is that chemical formulas of SOA products from OH-induced oxidation of cyclic and acyclic monoterpene mixtures can be adequately represented as a linear combination of contributions from individual VOCs. Indeed, SOA produced from β-myrcene/D-limonene mixtures appears to be dominated by chemical formulas that are also observed in the pure single-component systems, with only a small contribution from formulas that are unique to mixtures of VOCs. When analyzing EICs of specific ions in more detail, distinct isomers do emerge in the mixture SOA, confirming product formation pathways that are unique to the mixtures of VOCs. However, one must keep in mind that these mixture-specific products can be expected only under relatively high concentrations of VOCs or oxidants when $RO_2 + R'O_2$ and other types of dimer-forming reactions become significant. Under most actual atmospheric conditions, wherein the RO_2 concentrations are markedly lower than in the reaction chambers, the RO_2 isomerization and reactions of RO_2 with HO_2 or NO prevail, leading to minimal cross-products, even when complex mixtures of VOCs are oxidized.

As the impacts of climate change escalate, environmental stressors prompt plants to modify their BVOC emission profiles. Our experiments showed that an increased concentration of acyclic terpenes consistently produced greater SOA yields than cyclic terpenes. Owing to its additional reaction site and heightened reactivity, β-myrcene is observed to have higher efficiency at making SOA. Our finding highlights the need for more investigations on acyclic terpene mixtures in the context of changing climate.

https://doi.org/10.1021/acs.est.4c04870
Environ. Sci. Technol. 2024, 58, 13391−13401

■ ASSOCIATED CONTENT

Supporting Information

The Supporting Information is available free of charge at https://pubs.acs.org/doi/10.1021/acs.est.4c04870.

Parameters used for estimation of glass-transition temperature and saturation vapor pressure based on molecular formulas; comparison of EICs for major selected ions; comparison of observed and GECKO-A predicted mass spectra, number of isomeric species predicted by GECKO-A; scheme illustrating efficient formation of highly oxidized species during oxidation of β-myrcene; SOA yield from mixtures of β-myrcene and D-limonene (PDF)

■ AUTHOR INFORMATION

Corresponding Author

Sergey A. Nizkorodov − *Department of Chemistry, University of California Irvine, Irvine, California 92697, United States;* orcid.org/0000-0003-0891-0052; Email: nizkorod@uci.edu

Authors

Sijia Liu − *Department of Chemistry, University of California Irvine, Irvine, California 92697, United States;* orcid.org/0000-0002-6958-2868

Tommaso Galeazzo − *Department of Chemistry, University of California Irvine, Irvine, California 92697, United States;* orcid.org/0000-0001-9635-5460

Richard Valorso − *Univ Paris Est Creteil and Université Paris Cité, CNRS, LISA, Créteil F-94010, France*

Manabu Shiraiwa − *Department of Chemistry, University of California Irvine, Irvine, California 92697, United States;* orcid.org/0000-0003-2532-5373

Celia L. Faiola − *Department of Chemistry and Department of Ecology and Evolutionary Biology, University of California Irvine, Irvine, California 92697, United States;* orcid.org/0000-0002-4987-023X

Complete contact information is available at: https://pubs.acs.org/10.1021/acs.est.4c04870

Author Contributions

S.A.N. and C.L.F. developed the project idea and contributed to data synthesis and interpretation. S.L. conducted the experiments and data analysis and drafted the manuscript. T.G., R.V., and M.S. conducted GECKO-A modeling. The manuscript was edited through the contributions of all authors. All authors have given approval for the final version of the manuscript.

Funding

This work was supported by the National Science Foundation grants AGS-2035125 (L.L. and C.L.F.), AGS-2334731 (S.N.), and US Department of Energy grant DE-SC0022139 (T.G. and M.S.).

Notes

The authors declare no competing financial interest.

■ ACKNOWLEDGMENTS

The authors would like to thank Dr. Veronique Perraud for training on UPLC-ESI-HRMS and PTR-ToF-MS, Dr. Natalie R. Smith for useful discussion, Dr. Alex Guenther and Hui Wang for help with preparation of GC cartridges, Dr. Bernard Aumont and Dr. Marie Camredon for help with GECKO-A, and Shan Gu for her help on operating TD-GC-MS and useful discussion.

■ REFERENCES

(1) Hodzic, A.; Kasibhatla, P. S.; Jo, D. S.; Cappa, C. D.; Jimenez, J. L.; Madronich, S.; Park, R. J. Rethinking the Global Secondary Organic Aerosol (SOA) Budget: Stronger Production, Faster Removal. *Shorter Lifetime. Atmos. Chem. Phys.* **2016**, *16*, 7917−7941.

(2) Hallquist, M.; Wenger, J. C.; Baltensperger, U.; Rudich, Y.; Simpson, D.; Claeys, M.; Dommen, J.; Donahue, N. M.; George, C.; Goldstein, A. H.; Hamilton, J. F.; Herrmann, H.; Hoffmann, T.; Iinuma, Y.; Jang, M.; Jenkin, M. E.; Jimenez, J. L.; Kiendler-Scharr, A.; Maenhaut, W.; McFiggans, G.; Mentel, T. F.; Monod, A.; Prévôt, A. S. H.; Seinfeld, J. H.; Surratt, J. D.; Szmigielski, R.; Wildt, J. The Formation, Properties and Impact of Secondary Organic Aerosol: Current and Emerging Issues. *Atmos. Chem. Phys.* **2009**, *9* (14), 5155−5236.

(3) Spracklen, D. V.; Jimenez, J. L.; Carslaw, K. S.; Worsnop, D. R.; Evans, M. J.; Mann, G. W.; Zhang, Q.; Canagaratna, M. R.; Allan, J.; Coe, H.; McFiggans, G.; Rap, A.; Forster, P. Aerosol Mass Spectrometer Constraint on the Global Secondary Organic Aerosol Budget. *Atmos. Chem. Phys.* **2011**, *11* (23), 12109−12136.

(4) Liu, Y.; Dong, X.; Wang, M.; Emmons, L. K.; Liu, Y.; Liang, Y.; Li, X.; Shrivastava, M. Analysis of Secondary Organic Aerosol Simulation Bias in the Community Earth System Model (CESM2.1). *Atmos. Chem. Phys.* **2021**, *21* (10), 8003−8021.

(5) Zhu, J.; Penner, J. E.; Yu, F.; Sillman, S.; Andreae, M. O.; Coe, H. Decrease in Radiative Forcing by Organic Aerosol Nucleation, Climate, and Land Use Change. *Nature Commun.* **2019**, *10* (1), 1−7.

(6) Gu, S.; Guenther, A.; Faiola, C. Effects of Anthropogenic and Biogenic Volatile Organic Compounds on Los Angeles Air Quality. *Environ. Sci. Technol.* **2021**, *55* (18), 12191−12201.

(7) Kansal, A. Sources and Reactivity of NMHCs and VOCs in the Atmosphere: A Review. *J. Haz. Mat.* **2009**, *166* (1), 17−26.

(8) Roldin, P.; Liao, L.; Mogensen, D.; Dal Maso, M.; Rusanen, A.; Kerminen, V.-M.; Mentel, T. F.; Wildt, J.; Kleist, E.; Kiendler-Scharr, A.; Tillmann, R.; Ehn, M.; Kulmala, M.; Boy, M. Modelling the Contribution of Biogenic VOCs to New Particle Formation Modelling the Contribution of Biogenic VOCs to New Particle Formation in the Jülich Plant Atmosphere Chamber Modelling the Contribution of Biogenic VOCs to New Particle Formation. *Atmos. Chem. Phys.* **2015**, *15*, 10777−10798.

(9) Thompson, A. M. The Oxidizing Capacity of the Earth's Atmosphere: Probable Past and Future Changes. *Science* **1992**, *256* (5060), 1157−1165.

(10) Odum, J. R.; Hoffmann, T.; Bowman, F.; Collins, D.; Flagan, R. C.; Seinfeld, J. H. Gas/Particle Partitioning and Secondary Organic Aerosol Yields. *Environ. Sci. Technol.* **1996**, *30* (8), 2580−2585.

(11) Jang, M.; Czoschke, N. M.; Northcross, A. L.; Cao, G.; Shaof, D. SOA Formation from Partitioning and Heterogeneous Reactions: Model Study in the Presence of Inorganic Species. *Environ. Sci. Technol.* **2006**, *40* (9), 3013−3022.

(12) Zaveri, R. A.; Barnard, J. C.; Easter, R. C.; Riemer, N.; West, M. Particle-Resolved Simulation of Aerosol Size, Composition, Mixing State, and the Associated Optical and Cloud Condensation Nuclei Activation Properties in an Evolving Urban Plume. *J. Geophys.Res.: Atmospheres* **2010**, *115* (D17), 17210.

(13) Spracklen, D. V.; Carslaw, K. S.; Kulmala, M.; Kerminen, V. M.; Sihto, S. L.; Riipinen, I.; Merikanto, J.; Mann, G. W.; Chipperfield, M. P.; Wiedensohler, A.; Birmili, W.; Lihavainen, H. Contribution of Particle Formation to Global Cloud Condensation Nuclei Concentrations. *Geophys. Res. Lett.* **2008**, *35* (6), No. GL033038.

(14) Liang, C. W.; Chang, C. C.; Liang, J. J. The Impacts of Air Quality and Secondary Organic Aerosols Formation on Traffic Accidents in Heavy Fog−Haze Weather. *Heliyon* **2023**, *9* (4), No. e14631.

(15) Liu, L.; Kuang, Y.; Zhai, M.; Xue, B.; He, Y.; Tao, J.; Luo, B.; Xu, W.; Tao, J.; Yin, C.; Li, F.; Xu, H.; Deng, T.; Deng, X.; Tan, H.; Shao, M. Strong Light Scattering of Highly Oxygenated Organic Aerosols Impacts Significantly on Visibility Degradation. *Atmos. Chem.Phys.* **2022**, *22* (11), 7713−7726.
(16) Shiraiwa, M.; Ueda, K.; Pozzer, A.; Lammel, G.; Kampf, C. J.; Fushimi, A.; Enami, S.; Arangio, A. M.; Fröhlich-Nowoisky, J.; Fujitani, Y.; Furuyama, A.; Lakey, P. S. J.; Lelieveld, J.; Lucas, K.; Morino, Y.; Pöschl, U.; Takahama, S.; Takami, A.; Tong, H.; Weber, B.; Yoshino, A.; Sato, K. Aerosol Health Effects from Molecular to Global Scales. *Environ. Sci. Technol.* **2017**, *51* (23), 13545−13567.
(17) National Research Council (U.S.). Committee on Research Priorities for Airborne Particulate Matter. In *Research Priorities for Airborne Particulate Matter. IV, Continuing Research Progress*; 2004; p 355.
(18) Zhang, R.; Wang, G.; Guo, S.; Zamora, M. L.; Ying, Q.; Lin, Y.; Wang, W.; Hu, M.; Wang, Y. Formation of Urban Fine Particulate Matter. *Chem. Rev.* **2015**, *115* (10), 3803−3855.
(19) Faiola, C. L.; Buchholz, A.; Kari, E.; Yli-Pirilä, P.; Holopainen, J. K.; Kivimäenpää, M.; Miettinen, P.; Worsnop, D. R.; Lehtinen, K. E. J.; Guenther, A. B.; Virtanen, A. Terpene Composition Complexity Controls Secondary Organic Aerosol Yields from Scots Pine Volatile Emissions. *Sci. Rep.* **2018**, *8* (1), 1−13.
(20) Guenther, A.; Geron, C.; Pierce, T.; Lamb, B.; Harley, P.; Fall, R. Natural Emissions of Non-Methane Volatile Organic Compounds, Carbon Monoxide, and Oxides of Nitrogen from North America. *Atmos. Environ.* **2000**, *34* (12−14), 2205−2230.
(21) Guenther, A.; Hewitt, C. N.; Erickson, D.; Fall, R.; Geron, C.; Graedel, T.; Harley, P.; Klinger, L.; Lerdau, M.; Mckay, W. A.; Pierce, T.; Scholes, B.; Steinbrecher, R.; Tallamraju, R.; Taylor, J.; Zimmerman, P. A Global Model of Natural Volatile Organic Compound Emissions. *J. Geophys. Res.: Atmospheres* **1995**, *100* (D5), 8873−8892.
(22) Laothawornkitkul, J.; Taylor, J. E.; Paul, N. D.; Hewitt, C. N. Biogenic Volatile Organic Compounds in the Earth System: Tansley Review. *New Phytologist* **2009**, *183* (1), 27−51.
(23) Guenther, A.; Zimmerman, P.; Wildermuth, M. Natural Volatile Organic Compound Emission Rate Estimates for U.S. Woodland Landscapes. *Atmos. Environ.* **1994**, *28* (6), 1197−1210.
(24) Cao, J.; Situ, S.; Hao, Y.; Xie, S.; Li, L. Enhanced Summertime Ozone and SOA from Biogenic Volatile Organic Compound (BVOC) Emissions Due to Vegetation Biomass Variability during 1981−2018 in China. *Atmos.Chem. Phys.* **2022**, *22* (4), 2351−2364.
(25) Vedel-Petersen, I.; Schollert, M.; Nymand, J.; Rinnan, R. Volatile Organic Compound Emission Profiles of Four Common Arctic Plants. *Atmos. Environ.* **2015**, *120*, 117−126.
(26) Yang, W.; Zhang, B.; Wu, Y.; Liu, S.; Kong, F.; Li, L. Effects of Soil Drought and Nitrogen Deposition on BVOC Emissions and Their O_3 and SOA Formation for Pinus Thunbergii. *Environ. Pollut.* **2023**, *316* (Pt 2), No. 120693.
(27) Ghirardo, A.; Xie, J.; Zheng, X.; Wang, Y.; Grote, R.; Block, K.; Wildt, J.; Mentel, T.; Kiendler-Scharr, A.; Hallquist, M.; Butterbach-Bahl, K.; Schnitzler, J. P. Urban Stress-Induced Biogenic VOC Emissions and SOA-Forming Potentials in Beijing. *Atmos. Chem. Phys.* **2016**, *16* (5), 2901−2920.
(28) Liu, Y.; Schallhart, S.; Tykkä, T.; Räsänen, M.; Merbold, L.; Hellén, H.; Pellikka, P. Biogenic Volatile Organic Compounds in Different Ecosystems in Southern Kenya. *Atmos. Environ.* **2021**, *246*, No. 118064.
(29) Kiendler-Scharr, A.; Wildt, J.; Maso, M. D.; Hohaus, T.; Kleist, E.; Mentel, T. F.; Tillmann, R.; Uerlings, R.; Schurr, U.; Wahner, A. New Particle Formation in Forests Inhibited by Isoprene Emissions. *Nature* **2009**, *461* (7262), 381−384.
(30) Lee, S. H.; Uin, J.; Guenther, A. B.; de Gouw, J. A.; Yu, F.; Nadykto, A. B.; Herb, J.; Ng, N. L.; Koss, A.; Brune, W. H.; Baumann, K.; Kanawade, V. P.; Keutsch, F. N.; Nenes, A.; Olsen, K.; Goldstein, A.; Ouyang, Q. Isoprene Suppression of New Particle Formation: Potential Mechanisms and Implications. *J. Geophys. Res.: Atmospheres* **2016**, *121* (24), 14621−14635.
(31) Kanawade, V. P.; Jobson, B. T.; Guenther, A. B.; Erupe, M. E.; Pressley, S. N.; Tripathi, S. N.; Lee, S. H. Isoprene Suppression of New Particle Formation in a Mixed Deciduous Forest. *Atmos.Chem. Phys.* **2011**, *11* (12), 6013−6027.
(32) McFiggans, G.; Mentel, T. F.; Wildt, J.; Pullinen, I.; Kang, S.; Kleist, E.; Schmitt, S.; Springer, M.; Tillmann, R.; Wu, C.; Zhao, D.; Hallquist, M.; Faxon, C.; Le Breton, M.; Hallquist, Å. M.; Simpson, D.; Bergström, R.; Jenkin, M. E.; Ehn, M.; Thornton, J. A.; Alfarra, M. R.; Bannan, T. J.; Percival, C. J.; Priestley, M.; Topping, D.; Kiendler-Scharr, A. Secondary Organic Aerosol Reduced by Mixture of Atmospheric Vapours. *Nature* **2019**, *565* (7741), 587−593.
(33) Nie, W.; Yan, C.; Yang, L.; Roldin, P.; Liu, Y.; Vogel, A. L.; Molteni, U.; Stolzenburg, D.; Finkenzeller, H.; Amorim, A.; Bianchi, F.; Curtius, J.; Dada, L.; Draper, D. C.; Duplissy, J.; Hansel, A.; He, X. C.; Hofbauer, V.; Jokinen, T.; Kim, C.; Lehtipalo, K.; Nichman, L.; Mauldin, R. L.; Makhmutov, V.; Mentler, B.; Mizelli-Ojdanic, A.; Petäjä, T.; Quéléver, L. L. J.; Schallhart, S.; Simon, M.; Tauber, C.; Tomé, A.; Volkamer, R.; Wagner, A. C.; Wagner, R.; Wang, M.; Ye, P.; Li, H.; Huang, W.; Qi, X.; Lou, S.; Liu, T.; Chi, X.; Dommen, J.; Baltensperger, U.; El Haddad, I.; Kirkby, J.; Worsnop, D.; Kulmala, M.; Donahue, N. M.; Ehn, M.; Ding, A. NO at Low Concentration Can Enhance the Formation of Highly Oxygenated Biogenic Molecules in the Atmosphere. *Nature Commun.* **2023**, *14* (1), 1−11.
(34) Yan, C.; Nie, W.; Voge, A. L.; Dada, L.; Lehtipa, K.; Stolzenburg, D.; Wagner, R.; Rissanen, M. P.; Xiao, M.; Ahonen, L.; Fischer, L.; Rose, C.; Bianchi, F.; Gordon, H.; Simon, M.; Heinritzi, M.; Garmash, O.; Roldin, P.; Dias, A.; Ye, P.; Hofbauer, V.; Amorim, A.; Bauer, P. S.; Bergen, A.; Bernhammer, A. K.; Breitenlechner, M.; Brilke, S.; Buchholz, A.; Mazon, S. B.; Canagaratna, M. R.; Chen, X.; Ding, A.; Dommen, J.; Draper, D. C.; Duplissy, J.; Frege, C.; Heyn, C.; Guida, R.; Hakala, J.; Heikkinen, L.; Hoyle, C. R.; Jokinen, T.; Kangasluoma, J.; Kirkby, J.; Kontkanen, J.; Kürten, A.; Lawler, M. J.; Mai, H.; Mathot, S.; Mauldin, R. L., III; Molteni, U.; Nichman, L.; Nieminen, T.; Nowak, J.; Ojdanic, A.; Onnela, A.; Pajunoja, A.; Petäjä, T.; Piel, F.; Quéléver, L. L. J.; Sarnela, N.; Schallhart, S.; Sengupta, K.; Sipilä, M.; Tomé, A.; Tröst, J.; Vaïsänen, O.; Wagner, A. C.; Ylisirniö, A.; Zha, Q.; Baltensperger, U.; Carslaw, K. S.; Curtius, J.; Flagan, R. C.; Hanse, A.; Riipinen, I.; Smith, J. N.; Virtanen, A.; Winkler, P. M.; Donahue, N. M.; Kerminen, V. M.; Kulmala, M.; Ehn, M.; Worsnop, D. R. Size-Dependent Influence of Nox on the Growth Rates of Organic Aerosol Particles. *Sci. Adv.* **2020**, *6* (22), 4945−4972.
(35) Lehtipalo, K.; Yan, C.; Dada, L.; Bianchi, F.; Xiao, M.; Wagner, R.; Stolzenburg, D.; Ahonen, L. R.; Amorim, A.; Baccarini, A.; Bauer, P. S.; Baumgartner, B.; Bergen, A.; Bernhammer, A. K.; Breitenlechner, M.; Brilke, S.; Buchholz, A.; Mazon, S. B.; Chen, D.; Chen, X.; Dias, A.; Dommen, J.; Draper, D. C.; Duplissy, J.; Ehn, M.; Finkenzeller, H.; Fischer, L.; Frege, C.; Fuchs, C.; Garmash, O.; Gordon, H.; Hakala, J.; He, X.; Heikkinen, L.; Heinritzi, M.; Helm, J. C.; Hofbauer, V.; Hoyle, C. R.; Jokinen, T.; Kangasluoma, J.; Kerminen, V. M.; Kim, C.; Kirkby, J.; Kontkanen, J.; Kürten, A.; Lawler, M. J.; Mai, H.; Mathot, S.; Mauldin, R. L.; Molteni, U.; Nichman, L.; Nie, W.; Nieminen, T.; Ojdanic, A.; Onnela, A.; Passananti, M.; Petäjä, T.; Piel, F.; Pospisilova, V.; Quéléver, L. L. J.; Rissanen, M. P.; Rose, C.; Sarnela, N.; Schallhart, S.; Schuchmann, S.; Sengupta, K.; Simon, M.; Sipilä, M.; Tauber, C.; Tomé, A.; Tröstl, J.; Väisänen, O.; Vogel, A. L.; Volkamer, R.; Wagner, A. C.; Wang, M.; Weitz, L.; Wimmer, D.; Ye, P.; Ylisirniö, A.; Zha, Q.; Carslaw, K. S.; Curtius, J.; Donahue, N. M.; Flagan, R. C.; Hansel, A.; Riipinen, I.; Virtanen, A.; Winkler, P. M.; Baltensperger, U.; Kulmala, M.; Worsnop, D. R. Multicomponent New Particle Formation from Sulfuric Acid, Ammonia, and Biogenic Vapors. *Sci. Adv.* **2018**, *4* (12), No. eaau5363.
(36) Dada, L.; Stolzenburg, D.; Simon, M.; Fischer, L.; Heinritzi, M.; Wang, M.; Xiao, M.; Vogel, A. L.; Ahonen, L.; Amorim, A.; Baalbaki, R.; Baccarini, A.; Baltensperger, U.; Bianchi, F.; Daellenbach, K. R.; DeVivo, J.; Dias, A.; Dommen, J.; Duplissy, J.; Finkenzeller, H.; Hansel, A.; He, X. C.; Hofbauer, V.; Hoyle, C. R.; Kangasluoma, J.; Kim, C.; Kürten, A.; Kvashnin, A.; Mauldin, R.; Makhmutov, V.;

https://doi.org/10.1021/acs.est.4c04870
Environ. Sci. Technol. 2024, 58, 13391−13401

Marten, R.; Mentler, B.; Nie, W.; Petäjä, T.; Quéléver, L. L. J.; Saathoff, H.; Tauber, C.; Tome, A.; Molteni, U.; Volkamer, R.; Wagner, R.; Wagner, A. C.; Wimmer, D.; Winkler, P. M.; Yan, C.; Zha, Q.; Rissanen, M.; Gordon, H.; Curtius, J.; Worsnop, D. R.; Lehtipalo, K.; Donahue, N. M.; Kirkby, J.; El Haddad, I.; Kulmala, M. Role of Sesquiterpenes in Biogenic New Particle Formation. *Sci. Adv.* **2023**, *9* (36), No. eadi5297.

(37) Takeuchi, M.; Berkemeier, T.; Eris, G.; Ng, N. L. Non-Linear Effects of Secondary Organic Aerosol Formation and Properties in Multi-Precursor Systems. *Nature Commun.* **2022**, *13* (1), 1−13.

(38) Niinemets, Ü.; Kännaste, A.; Copolovici, L. Quantitative Patterns between Plant Volatile Emissions Induced by Biotic Stresses and the Degree of Damage. *Frontiers. Plant Sci.* **2013**, *4* (JUL), 49750.

(39) Holopainen, J. K.; Gershenzon, J. Multiple Stress Factors and the Emission of Plant VOCs. *Trends Plant Sci.* **2010**, *15* (3), 176−184.

(40) Faiola, C. L.; Pullinen, I.; Buchholz, A.; Khalaj, F.; Ylisirniö, A.; Kari, E.; Miettinen, P.; Holopainen, J. K.; Kivimäenpää, M.; Schobesberger, S.; Yli-Juuti, T.; Virtanen, A. Secondary Organic Aerosol Formation from Healthy and Aphid-Stressed Scots Pine Emissions. *ACS Earth and Space Chem.* **2019**, *3* (9), 1756−1772.

(41) Ylisirniö, A.; Buchholz, A.; Mohr, C.; Li, Z.; Barreira, L.; Lambe, A.; Faiola, C.; Kari, E.; Yli-Juuti, T.; Nizkorodov, S. A.; Worsnop, D. R.; Virtanen, A.; Schobesberger, S. Composition and Volatility of Secondary Organic Aerosol (SOA) Formed from Oxidation of Real Tree Emissions Compared to Simplified Volatile Organic Compound (VOC) Systems. *Atmos. Chem. Phys.* **2020**, *20* (9), 5629−5644.

(42) Heinritzi, M.; Dada, L.; Simon, M.; Stolzenburg, D.; Wagner, A. C.; Fischer, L.; Ahonen, L. R.; Amanatidis, S.; Baalbaki, R.; Baccarini, A.; Bauer, P. S.; Baumgartner, B.; Bianchi, F.; Brilke, S.; Chen, D.; Chiu, R.; Dias, A.; Dommen, J.; Duplissy, J.; Finkenzeller, H.; Frege, C.; Fuchs, C.; Garmash, O.; Gordon, H.; Granzin, M.; El Haddad, I.; He, X.; Helm, J.; Hofbauer, V.; Hoyle, C. R.; Kangasluoma, J.; Keber, T.; Kim, C.; Kürten, A.; Lamkaddam, H.; Laurila, T. M.; Lampilahti, J.; Lee, C. P.; Lehtipalo, K.; Leiminger, M.; Mai, H.; Makhmutov, V.; Manninen, H. E.; Marten, R.; Mathot, S.; Mauldin, R. L.; Mentler, B.; Molteni, U.; Müller, T.; Nie, W.; Nieminen, T.; Onnela, A.; Partoll, E.; Passananti, M.; Petäje, T.; Pfeifer, J.; Pospisilova, V.; Quéléver, L. L. J.; Rissanen, M. P.; Rose, C.; Schobesberger, S.; Scholz, W.; Scholze, K.; Sipile, M.; Steiner, G.; Stozhkov, Y.; Tauber, C.; Tham, Y. J.; Vazquez-Pufleau, M.; Virtanen, A.; Vogel, A. L.; Volkamer, R.; Wagner, R.; Mingyi, W.; Lena, W.; Daniela, W.; Xiao, M.; Yan, C.; Ye, P.; Zha, Q.; Zhou, X.; Amorim, A.; Baltensperger, U.; Hansel, A.; Kulmala, M.; Tome, A.; Winkler, P. M.; Worsnop, D. R.; Donahue, N. M.; Kirkby, J.; Curtius, J. Molecular Understanding of the Suppression of New-Particle Formation by Isoprene. *Atmos. Chem. Phys.* **2020**, *20* (20), 11809−11821.

(43) Kourtchev, I.; Bejan, I.; Sodeau, J. R.; Wenger, J. C. Gas Phase Reaction of OH Radicals with (E)-β-Farnesene at 296 ± 2 K: Rate Coefficient and Carbonyl Products. *Atmos. Environ.* **2012**, *46*, 338−345.

(44) Rothfuss, N. E.; Petters, M. D. Influence of Functional Groups on the Viscosity of Organic Aerosol. *Environ. Sci. Technol.* **2017**, *51* (1), 271−279.

(45) Grayson, J. W.; Song, M.; Evoy, E.; Upshur, M. A.; Ebrahimi, M.; Geiger, F. M.; Thomson, R. J.; Bertram, A. K.; Bertram, A. Effect of Adding Hydroxyl Functional Groups and Increasing Molar Mass on the Viscosity of Organics Relevant to Secondary Organic Aerosols. *Atmos. Chem. Phys.* **2017**, *17*, 8509−8524.

(46) Atkinson, R.; Atkinson, R. Gas-Phase Tropospheric Chemistry of Volatile Organic Compounds: 1. Alkanes and Alkenes. *J. Phys. Chem. Ref. Data* **1997**, *26* (2), 215−290.

(47) Schum, S. K.; Brown, L. E.; Mazzoleni, L. R. MFAssignR: Molecular Formula Assignment Software for Ultrahigh Resolution Mass Spectrometry Analysis of Environmental Complex Mixtures. *Environ. Res.* **2020**, *191*, No. 110114.

(48) Aumont, B.; Szopa, S.; Madronich, S. Modelling the Evolution of Organic Carbon during Its Gas-Phase Tropospheric Oxidation: Development of an Explicit Model Based on a Self Generating Approach. *Atmos. Chem. Phys.* **2005**, *5* (9), 2497−2517.

(49) Schervish, M.; Donahue, N. M. Peroxy Radical Chemistry and the Volatility Basis Set. *Atmos. Chem. Phys.* **2020**, *20* (2), 1183−1199.

(50) Romonosky, D. E.; Laskin, A.; Laskin, J.; Nizkorodov, S. A. High-Resolution Mass Spectrometry and Molecular Characterization of Aqueous Photochemistry Products of Common Types of Secondary Organic Aerosols. *J. Phys. Chem. A* **2015**, *119* (11), 2594−2606.

(51) Gallimore, P. J.; Mahon, B. M.; Wragg, F. P. H.; Fuller, S. J.; Giorio, C.; Kourtchev, I.; Kalberer, M. Multiphase Composition Changes and Reactive Oxygen Species Formation during Limonene Oxidation in the New Cambridge Atmospheric Simulation Chamber (CASC). *Atmos. Chem. Phys.* **2017**, *17* (16), 9853−9868.

(52) Luo, H.; Vereecken, L.; Shen, H.; Kang, S.; Pullinen, I.; Hallquist, M.; Fuchs, H.; Wahner, A.; Kiendler-Scharr, A.; Mentel, T. F.; Zhao, D. Formation of Highly Oxygenated Organic Molecules from the Oxidation of Limonene by OH Radical: Significant Contribution of H-Abstraction Pathway. *Atmos. Chem. Phys.* **2023**, *23*, 7297−7319.

(53) Thomsen, D.; Thomsen, L. D.; Iversen, E. M.; Björgvinsdóttir, T. N.; Vinther, S. F.; Skønager, J. T.; Hoffmann, T.; Elm, J.; Bilde, M.; Glasius, M. Ozonolysis of α-Pinene and Δ^3-Carene Mixtures: Formation of Dimers with Two Precursors. *Environ. Sci. Technol.* **2022**, *56* (23), 16643−16651.

(54) Schervish, M.; Shiraiwa, M. Impact of Phase State and Non-Ideal Mixing on Equilibration Timescales of Secondary Organic Aerosol Partitioning. *Atmos. Chem. Phys.* **2023**, *23* (1), 221−233.

(55) Zaveri, R. A.; Shilling, J. E.; Zelenyuk, A.; Liu, J.; Bell, D. M.; D'Ambro, E. L.; Gaston, C. J.; Thornton, J. A.; Laskin, A.; Lin, P.; Wilson, J.; Easter, R. C.; Wang, J.; Bertram, A. K.; Martin, S. T.; Seinfeld, J. H.; Worsnop, D. R. Growth Kinetics and Size Distribution Dynamics of Viscous Secondary Organic Aerosol. *Environ. Sci. Technol.* **2018**, *52* (3), 1191−1199.

(56) Zaveri, R. A.; Shilling, J. E.; Zelenyuk, A.; Zawadowicz, M. A.; Suski, K.; China, S.; Bell, D. M.; Veghte, D.; Laskin, A. Particle-Phase Diffusion Modulates Partitioning of Semivolatile Organic Compounds to Aged Secondary Organic Aerosol. *Environ. Sci. Technol.* **2020**, *54* (5), 2595−2605.

(57) Reid, J. P.; Bertram, A. K.; Topping, D. O.; Laskin, A.; Martin, S. T.; Petters, M. D.; Pope, F. D.; Rovelli, G. The Viscosity of Atmospherically Relevant Organic Particles. *Nature Communications 2018 9:1* **2018**, *9* (1), 1−14.

(58) Shiraiwa, M.; Ammann, M.; Koop, T.; Pöschl, U. Gas Uptake and Chemical Aging of Semisolid Organic Aerosol Particles. *Proc. Natl. Acad. Sci. U.S.A.* **2011**, *108* (27), 11003−11008.

(59) Wong, J. P. S.; Zhou, S.; Abbatt, J. P. D. Changes in Secondary Organic Aerosol Composition and Mass Due to Photolysis: Relative Humidity Dependence. *J. Phys. Chem. A* **2015**, *119* (19), 4309−4316.

(60) Li, Y.; Pöschl, U.; Shiraiwa, M. Molecular Corridors and Parameterizations of Volatility in the Chemical Evolution of Organic Aerosols. *Atmos. Chem. Phys.* **2016**, *16* (5), 3327−3344.

(61) DeRieux, W. S. W.; Li, Y.; Lin, P.; Laskin, J.; Laskin, A.; Bertram, A. K.; Nizkorodov, S. A.; Shiraiwa, M. Predicting the Glass Transition Temperature and Viscosity of Secondary Organic Material Using Molecular Composition. *Atmos. Chem. Phys.* **2018**, *18* (9), 6331−6351.

(62) Li, Y.; Day, D.; Stark, H.; Jimenez, J. L.; Shiraiwa, M. Predictions of the Glass Transition Temperature and Viscosity of Organic Aerosols from Volatility Distributions. *Atmos. Chem. Phys.* **2020**, *20* (13), 8103−8122.

(63) Jokinen, T.; Berndt, T.; Makkonen, R.; Kerminen, V. M.; Junninen, H.; Paasonen, P.; Stratmann, F.; Herrmann, H.; Guenther, A. B.; Worsnop, D. R.; Kulmala, M.; Ehn, M.; Sipilä, M. Production of Extremely Low Volatile Organic Compounds from Biogenic Emissions: Measured Yields and Atmospheric Implications. *Proc. Natl. Acad. Sci. U.S.A.* **2015**, *112* (23), 7123−7128.

(64) Bianchi, F.; Kurtén, T.; Riva, M.; Mohr, C.; Rissanen, M. P.; Roldin, P.; Berndt, T.; Crounse, J. D.; Wennberg, P. O.; Mentel, T. F.;

https://doi.org/10.1021/acs.est.4c04870
Environ. Sci. Technol. 2024, 58, 13391−13401

Wildt, J.; Junninen, H.; Jokinen, T.; Kulmala, M.; Worsnop, D. R.; Thornton, J. A.; Donahue, N.; Kjaergaard, H. G.; Ehn, M. Highly Oxygenated Organic Molecules (HOM) from Gas-Phase Autoxidation Involving Peroxy Radicals: A Key Contributor to Atmospheric Aerosol. *Chem. Rev.* **2019**, *119* (6), 3472−3509.
(65) Tong, H.; Zhang, Y.; Filippi, A.; Wang, T.; Li, C.; Liu, F.; Leppla, D.; Kourtchev, I.; Wang, K.; Keskinen, H. M.; Levula, J. T.; Arangio, A. M.; Shen, F.; Ditas, F.; Martin, S. T.; Artaxo, P.; Godoi, R. H. M.; Yamamoto, C. I.; De Souza, R. A. F.; Huang, R. J.; Berkemeier, T.; Wang, Y.; Su, H.; Cheng, Y.; Pope, F. D.; Fu, P.; Yao, M.; Pöhlker, C.; Petäjä, T.; Kulmala, M.; Andreae, M. O.; Shiraiwa, M.; Pöschl, U.; Hoffmann, T.; Kalberer, M. Radical Formation by Fine Particulate Matter Associated with Highly Oxygenated Molecules. *Environ. Sci. Technol.* **2019**, *53* (21), 12506−12518.
(66) Krapf, M.; El Haddad, I.; Bruns, E. A.; Molteni, U.; Daellenbach, K. R.; Prévôt, A. S. H.; Baltensperger, U.; Dommen, J. Labile Peroxides in Secondary Organic Aerosol. *Chem.* **2016**, *1* (4), 603−616.
(67) Pankow, J. F. An Absorption Model of Gas/Particle Partitioning of Organic Compounds in the Atmosphere. *Atmos. Environ.* **1994**, *28* (2), 185−188.

https://doi.org/10.1021/acs.est.4c04870
Environ. Sci. Technol. 2024, 58, 13391−13401